Facile Approach to Large-Scale Synthesis of 1D Calcium and Titanium Precipitate (CTP) with High Electrorheological Activity

Yuchuan Cheng,* Kaihua Wu, Fenghua Liu, Jianjun Guo, Xuehui Liu, Gaojie Xu, and Ping Cui

Ningbo Institute of Material Technology and Engineering, Chinese Academy of Sciences, Ningbo 315201, P. R. China

ABSTRACT Nanorods of calcium and titanium precipitate (CTP) were prepared via a simple precipitation route in an ethanol/water mixed solution system under mild conditions. The obtained rodlike particles were highly uniform in width (23 ± 3 nm), and its length could be tuned by adjusting the concentration of oxalic acid reactant. The nanorods materials show a promising electrorheological activity, of which ER efficiency was about 4 times higher that of granular CTP suspensions. The facile synthesis route may be regarded as a green chemistry method, and its novelty relies on the large-scale production of 1D CTP giant ER materials.

KEYWORDS: one-dimensional • electrorheological • large-scale • calcium and titanium precipitate

INTRODUCTION

Electrorheological (ER) fluids are a kind of smart suspension composed of polarizable solid particles dispersed in nonpolar liquid medium, which exhibit drastic changes in their rheological properties under an applied electric field (1−3). Because of their rapid response times, reversibility, simple mechanics, and low power consumption, ER fluids are regarded as potential materials for use in numerous electromechanical devices such as active devices, clutches, brakes, shock absorbers, etc. (4, 5). Nevertheless, the broad applications of ER devices have been hampered by the poor ER activity of most available ER fluids. Thus, improving the ER capability of ER fluids is of urgent significance for the further development of electromechanical industry.

Many recent studies show that the shape effect of particles could greatly affect the ER activity of materials (6, 7). Since the discovery of carbon nanotubes in 1991 (8), one-dimensional (1D) nanostructures (rods, wires, and tubes) have attracted extensive attention because of their fundamental significance in investigating the dependence of various physicochemical properties on dimensionality and size reduction, as well as potential applications in numerous fields (9−11). The applications of 1D nanomaterial in conventional ER fluids have been reported, in which nanotubes, nanowires, and nanowhiskers were dispersed in silicone oil. It is exciting that compared with spherical particles, 1D nanomaterials can enhance ER or magnetorheological (MR) effect of ER or MR fluids and even improve the dispersion stability (12−14). Giant ER fluids have received considerable attention after 2003. However, 1D structured giant ER materials are relatively undeveloped. Although there are well-established high-temperature strategies to control the morphologies of a broad class of inorganic materials including metals, metal oxides, and many other compounds (15−17), the synthesis of giant ER materials with controlled morphology is very difficult because of their multicomponent and low-temperature manufacture process. Therefore, it is still a challenge to develop an effective and facile pathway to fabricate highly ER active 1D giant ER materials.

Calcium and titanium precipitae (CTP) synthesized via oxalate route is one of the best giant ER material, which holds great potential for scalable applications (18, 19). The CTP powders prepared by conventional wet chemical method are submicrosized particles with irregular shape, wide size distribution, and serious aggregation, which limit their practical applications. In our earlier studies, we have optimized the precipitation conditions to get core−shell SiO_2−CTP nanoparticles with spherical morphology and narrow size distribution (20). Herein we report, for the first time, on the nanorods of CTP particles fabricated by a precipitation method that involves the $TiO(C_2O_4)^{2-}$ inhibition in an ethanol/water mixed solution system. The present approach can even be scaled up as a green chemistry method for the industrial production of the CTP giant ER materials. As much as 180 g of CTP nanorods can be obtained in one reaction (see Figure S1 in the Supporting Information).

EXPERIMENTAL SECTION

Chemicals. Tetrabutyl titanate (TBT, >98%), anhydrous calcium chloride ($CaCl_2$, A. R.), oxalic acid dihydrate ($H_2C_2O_4.2H_2O$, A. R.), HCl (37%, A. R.) and $NH_3 \cdot H_2O$ (25%, A. R.) were purchased from Sinopharm Chemical Reagent Company (Shanghai, China). Silicone oils (η = 10 mPa s) were obtained from Hangping Company (Beijing, China). All the chemicals cited above were used as received without further purification. The water used in this work was deionized (DI) water form a Millipor-Q purification system (Milli-

* To whom correspondence should be addressed. Phone: +86-574-86685162. Fax: +86-574-86685163. E-mail: yccheng@nimte.ac.cn.

Received for review November 30, 2009 and accepted February 11, 2010

DOI: 10.1021/am900841m

pore, USA) of resistivity 18.2 MΩ cm. All organic solvents used were of analytical grade and purchased from Sinopharm Chemical Reagent Company (Shanghai, China).

Synthesis Procedures. The CTP nanorods were synthesized by means of precipitation process. In a typical procedure, 15.9 mmol of oxalic acid were dissolved in 100 mL of ethanol/water (V/V = 1/1) solution. The solution was vigorous stirred for 1 h, and 0.063 mol/L solution of TBT made by dissolving 6.3 mmol of TBT in 100 mL of ethanol was slowly added under stirring. When the white precipitate initially obtained was redissolved, a clear solution a was obtained. The pH value of the solution a was then kept between 2 and 3 adjusted with by diluted ammonia. At same time, solution b was prepared by dissolving 6.5 mmol of calcium chloride in 50 mL of DI water. The pH of this solution was adjusted to 3−4 by adding diluted HCl. Solution b was then slowly dropped into solution a with rigorous stirring conditions at 40 °C. The opalescent precipitation was produced instantly and the mixture was stirred continuously for 30 min, followed by aging overnight at a constant temperature of 40 °C. The precipitate was centrifuged and washed with DI water and ethanol. It was then dehydrated in a vacuum at 60 °C for 12 h and at 110 °C for another 4 h. In the experiments, the oxalic acid dosage was varied from 12.8 to 18.9 mmol. The CTP prepared with oxalic acid dosage = 12.8, 14.6, 15.9, 17.7, 18.9 are identified as CTP12, CTP14, CTP15, CTP17, and CTP18, respectively.

All the silicone oils were dried at 120 °C for 2 h before the experiment to avoid the influence of moisture. The ER fluids were formed by mixed the CTP nanoparticles with silicone oils. Subsequently, the mixed suspension was dry at 60 °C for 1 h. Concentration of the ER fluids is denoted as the ratio of the solid particles weight to the total weight of the ER fluid.

To obtain hectogram-scale CTP nanorods, the concentrations and volumes of the reactants were multiplied 20 times in a 10 L vessel, whereas the other conditions were kept unchanged.

Characterization. X-ray diffraction (XRD) patterns were obtained with a Bruker D8 Advance/Discover diffractometer, using CuKα radiation. All measurements were taken using a generator voltage of 40 kV and a current of 40 mA. Component analysis was examined by Perkin-Elmer Optima 2100 inductively coupled plasma (ICP) spectrometer. Fourier transform infrared (FTIR) spectra were recorded on Nicolet 6700 spectrometer using 32 averaged scans at 4 cm^{-1} resolution. The solid samples were prepared as KBr pellets. The morphology and grain size of the samples were examined by a Hitachi S4800 field emission scanning election microscope (FESEM) and FEI Tecnai G2 F20 transmission electron microscope (TEM).

The static yield stress was measured by a circular-plate type rheometer (Haake RS6000, 15 mm in diameter). Experimental data were collected with the help of the software package Rheowin. The suspensions were placed in the gap between two plates separated by a distance of 1.00 ± 0.001 mm. The maximum voltage of the DC high-voltage generator (SPELLMAN SL300) was 10 kV, and the current limitation was 3.0 mA. The stress rate used for the static yield stress measurement was 0.1 s^{-1}. In our experiment, the static yield stress was determined by the maximum shear stress value at which a kink occurs in the stress-time curve. The shear stress vs shear rate curve of the ER suspensions was measured using the rotary cup accessory of Haake RS6000 rheometer. The gap between the outer cup and the inner bob is 1.0 mm. The rheological curves were measured in the CR mode within the shear rate range of 1−100 s^{-1}. Each shear rate was maintained for 30 s to ensure that the stationary state was reached. All measurements were carried out at room temperature.

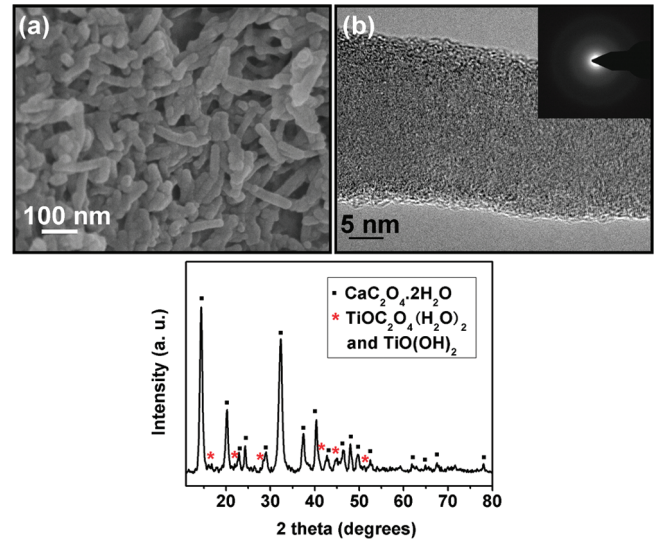

FIGURE 1. (a)SEM image, (b) TEM image, with the SAED pattern in the inset, and (bottom) XRD pattern of the CTP15 nanorods.

RESULTS AND DISCUSSION

The morphologies and microstructure of the samples were characterized by SEM, TEM, and XRD analysis. Figure 1a shows a SEM image of the as-dried CTP15 sample. The picture reveals that the sample consists of rod-like particles having rather uniform width of 23 ± 3 nm and length of 40−130 nm. The HRTEM image recorded from an individual nanorod (Figure 1b) displays the polycrystalline nature of the nanorod with the smooth surface. Continuous sharp circles on the SAED (small-angle electron diffraction) pattern (inset of Figure 1b) further confirms that the sample is composed of polycrystalline nanostructures. The corresponding XRD pattern is shown in Figure 1c. The calculated values of *d* match very well with the reported X-ray data for calcium oxalate dehydrate (COD) (JCPDS NO. 17−0541). Furthermore, the unidentified lines in XRD pattern are attributed to $TiOC_2O_4(H_2O)_2$ and $TiO(OH)_2$, as it is difficult to obtain crystalline precipitate of $TiOC_2O_4(H_2O)_2$ (21−23). To confirm further the component of CTP, the ICP and chemistry analysis on the CTP nanorods were carried out. The obtained results are given below

Ca = 12.03 wt %, Ti = 12.23 wt %, $C_2O_4^{2-}$ = 41.15 wt % (molar ratio:[Ca + Ti]/[$C_2O_4^{2-}$] = 2.2:1.8)

Thus, the main component of CTP is considered as $CaC_2O_4 \cdot 2H_2O$, $TiOC_2O_4(H_2O)_2$, and $TiO(OH)_2$. The following reaction scheme is suggested during synthesis and washing procedure.

$$Ti(C_4H_9O)_4 + 4H_2O \rightarrow TiO(OH)_2 \downarrow + 4C_4H_9OH \quad (1)$$

$$TiO(OH)_2 + 2H_2C_2O_4 \rightarrow TiO(C_2O_4)_2^{2-} + 2H^+ + 2H_2O \quad (2)$$

$$CaCl_2 \rightarrow Ca^{2+} + 2Cl^- \quad (3)$$

$$Ca^{2+} + C_2O_4^{2-} + 2H_2O \rightarrow CaC_2O_4 \cdot 2H_2O \downarrow \quad (4)$$

$$TiO(C_2O_4)_2^{2-} + 2H_2O \rightarrow TiOC_2O_4(H_2O)_2 \downarrow + C_2O_4^{2-} \quad (5)$$

$$TiO(C_2O_4)_2^{2-} + 2H_2O \rightarrow TiO(OH)_2 \downarrow + 2C_2O_4^{2-} + 2H^+ \quad (6)$$

It is well-known that calcium oxalate has a low solubility in semiaqueous media. When Ca^{2+} cations are added, the excessive $C_2O_4^{2-}$ anions are consumed to precipitate stable calcium oxalate compound by reaction 4. Simultaneously, $TiO(C_2O_4)^{2-}$ anions formed by reaction 2 are destabilized forming insoluble $TiOC_2O_4(H_2O)_2$ and $C_2O_4^{2-}$ anions (24). These in situ regenerated $C_2O_4^{2-}$ anions react continually with Ca^{2+} cations. When the precipitates are washed only by ethanol, the [Ca+Ti]/[$C_2O_4^{2-}$] ratio of the product is almost 1. Therefore, we suggest that a small amount titanium precipitates as hydroxide are formed from the residual $TiO(C_2O_4)^{2-}$ anions by the hydrolysis reaction 6 in the water washing step.

The above phase formation is further determined by FT-IR spectroscopy. In Figure 2, the large band centered at around 3438 cm^{-1} is assigned to the O−H stretching modes of interlayer water molecules. Similarly, a shoulder band at 2969 cm^{-1} from hydrogen bonding in the interlayer also is observed (25). The absorption bands at 1649 and 1324 cm^{-1} are assigned to the metal−carboxylate (M-COO^-) of calcium oxalate dihydrate (COD) asymmetric and symmetric stretching modes, respectively. The presence of COD is further confirmed by the presence of characteristic bands for COD at 613 cm^{-1} (26). The shoulder band at 769 cm^{-1} may originate from the adsorbed $TiO(C_2O_4)_2^{2-}$ anion, which indicates that $TiO(C_2O_4)_2^{2-}$ anions are present at the surface of the CTP15 nanorods. The band at 529 cm^{-1} is attributed

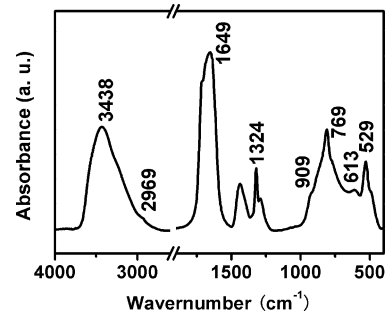

FIGURE 2. IR spectrum of the CTP15 nanorods.

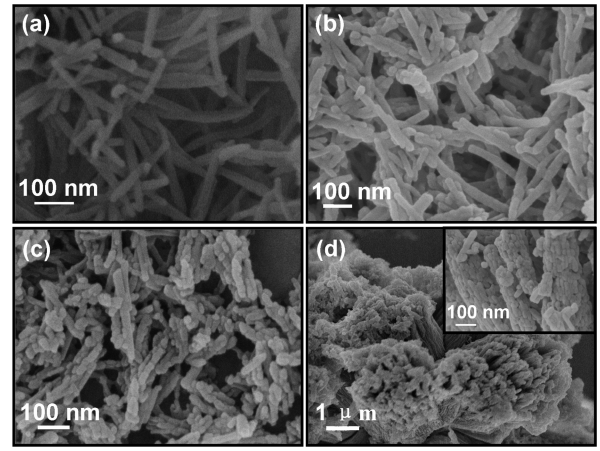

FIGURE 3. SEM images of the CTP particles precipitated at different OA dosage: (a) 12.8, (b) 14.6, (c) 17.7, and (d) 18.9, with the larger magnification in the inset (OA).

to the O−C−O in plane bending. Form the IR spectra, we also can observe a shoulder band at 909 cm^{-1} for Ti═O double bond, adding another evidence for the existence of $TiOC_2O_4(H_2O)_2$.

Varying the quantity of oxalic acid can lead to a morphological variation of the final products. When the Ca^{2+} and Ti^{4+} cation concentrations were maintained at 0.026 and 0.025 mol/L. At lower OA dosage of 12.8 mmol, a limited number of long CTP nanorods (length= 80−200 nm) are observed (Figure 3a). In comparison, high yields of progressively shorter nanorods are produced as the OA dosage is increased to 14.6 and 17.7 mmol, although the mean width remains unchanged (Figure 3b-c). When the OA dosage increases to 18.9 mmol, an unusual CTP nanostructure form is shown in the different magnification SEM images in Figure 3d. The low-magnification SEM image shows that flower-like CTP particles with a size ranging from about 3.0 μm. It is clearly shown that the flowerlike particles are constructed by rod clusters which are composed of short rods (width = 20 ± 5 nm, length = 30−60 nm) in the inset of Figure 3d. The above results illustrate that the $TiO(C_2O_4)^{2-}$ anions could act as not only an origin of $C_2O_4^{2-}$ anions but also an inhibitor that controls the growth process of particles during precipitation. The presence of the large numbers of $TiO(C_2O_4)^{2-}$ anions in solution that can be selectively adsorbed on the COD particles decreases the rate of particle growth in the direction of the side planes of the rod and suppress the particle aggregation. With the increase in the OA content, the number of primary COD particles increases,

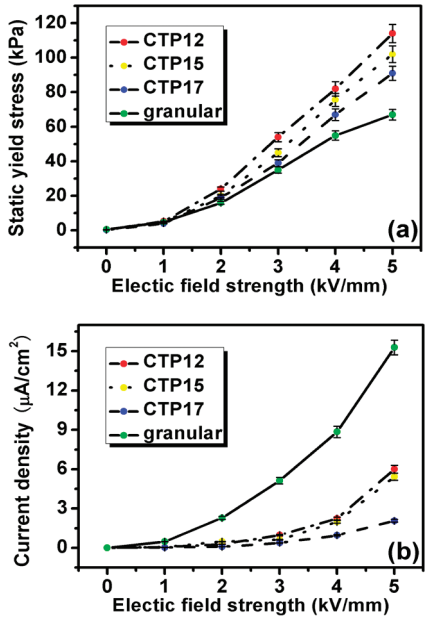

FIGURE 4. (a) Static yield stress and (b) current density of the rodlike CTP12, CTP15, CTP17, and granular CTP suspensions (66.6 wt %) as a function of applied electric field.

and therefore, high yields of shorter nanorods are produced. When the OA dosage is 18.9 mmol, the number of primary COD particles is much higher, and the inhibition of $TiO(C_2O_4)^{2-}$ anion is insufficient, which results in the formation of flowerlike particles.

CTP is an important ER-active material. Here, we investigated the ER capability of the rodlike CTP 12, CTP 15, CTP17 compared with the granular CTP particles. The shear stresses of the CTP ER fluid (37.5 wt %) as function of shear rate under various electric fields are shown in Figure S2 on the Supporting Information. Furthermore, the better ER capability of the rodlike CTP suspensions with high weight fraction when compare to the granular CTP suspension with same weight fraction is worth mentioning. Because of the measuring range limit of our rheometer, the shear stresses of the high weight fraction ER fluids could not be obtained. Therefore, we measured the static yield stresses of these ER fluids. Figure 4 shows the static yield stress and the current density of these CTP ER fluids under the different DC electric field (66.6 wt %). The static yield stress displays near-linear dependence of the electric field strength and the linearity starts at a critical field $E_c \approx 1$ kV/mm. It indicates a saturated polarization layer is established, which is the distinct feature of the giant ER fluids (27, 28). Obviously, all the rodlike samples have a higher static yield stress than that of the granular sample. Under electric fields, the CTP12 ER fluid exhibits the strongest yield stress (114 kPa, 5 kV/mm). We consider that different shape of the CTP particle results in different ER capability. It has been reported that the elongated particles in electric field tend to combine into dendrite-like network structure that is firmer than the chainlike structure formed by the spherical particles (12). Furthermore, the head-to-head configuration of two elongated particles gives enhanced local electric field, which leads to larger induced dipole moments and interparticle interactions than those of the spherical particles of same volume in electric field (29, 30). Therefore, the rodlike CTP suspensions possess high yield stress. The ER efficiency is defined by $(\tau_E - \tau_0)/\tau_0$, where τ_E is the static yield stress with an electric field, and τ_0 is the static yield stress at zero field. The ER efficiency for the CTP12, CTP15, CTP17 suspensions, and the granular CTP suspension is 264, 485, 454, and 125, respectively. The CTP 15 suspension has the highest ER efficiency, which could be explained as follows. On the one hand, the high aspect ratio makes high yield stress at electric field. On the other hand, as the aspect ratio of particle is increased, the yield stress at zero electric field increases, too. The CTP15 sample has a moderate aspect ratio. Consequently, the CTP15 suspensions showed the comparatively high yield stress at electric field, comparatively low yield stress at zero electric field, and highest ER efficiency that was 3.8 times as high as that of granular CTP suspension. The current density of ER fluid is regarded as the other main factor in practical application, because the ER fluids with higher current density will consume more power. In Figure 4b, we can note that the current density of the rodlike CTP suspensions are below 7 $\mu A/cm^2$ at 5 kV/mm, whereas the corresponding current density of the granular CTP ER fluid is about 15 $\mu A/cm^2$. The result means the bond between ions in the CTP nanorods is stronger than that in granular CTP.

CONCLUSION

In summary, we successfully carried out the large-scale of synthesis of the CTP nanorods through a facile precipitation route in an ethanol/water mixed solution system without using any surfactant. The concentration-dependent products study confirms that the shape evolution could be driven by the $TiO(C_2O_4)^{2-}$ anions. These prepared rodlike CTP nanoparticles clearly show an exhibit ER activity that outclasses that of granular CTP nanoparticles. This paper provides a simple and effective strategy for the frabrication of 1D giant ER mateirals.

Acknowledgment. This project is financially supported by the Ningbo Natural Science Foundation, Zhejiang Provincial Natural Science Foundation of China (Y4090044), the National Basic Research Program of China (2009CB930801), the Fund of Chinese Academy of Sciences (KJCX2.YW.M07), and Zhejiang Natural Science Fund (D4080489).

Supporting Information Available: More details of the sample characterization including photo of hectogram-scale powder of CTP nanorods, shear stress vs shear rate curves of the CTP ER fluid, and SEM image of the granular CTP particles (PDF). This material is available free of charge via the Internet at http://pubs.acs.org.

REFERENCES AND NOTES

(1) Winslow, W. M. *J. Appl. Phys.* **1949**, *20*, 1137–1140.
(2) Halsey, T. C. *Science* **1992**, *258*, 761–766.
(3) Klingenberg, D. J.; Zukoski, C. F. *Langmuir* **1990**, *6*, 15–24.
(4) Hyun, Y. H.; Lim, S. T.; Choi, H. J.; Jhon, M. S. *Macromolecules* **2001**, *34*, 8084–8093.
(5) Espin, M. J.; Delgado, A. V.; Plocharski, J. *Langmuir* **2005**, *21*, 4896–4903.
(6) Wang, B. X.; Zhao, X. P. *Adv. Funct. Mater.* **2005**, *15*, 1815–1820.

(7) Kanu, R. C.; Shaw, M. T. *J. Rheol.* **1998**, *42*, 657–670.
(8) Iijima, S. *Nature* **1991**, *354*, 56–58.
(9) Hu, J. T.; Odom, T. W.; Lieber, C. M. *Acc. Chem. Res.* **1999**, *32*, 435–445.
(10) Whitesides, G. M.; Grzybowski, B. *Science* **2002**, *295*, 2418–2421.
(11) Mieszawska, A. J.; Slawinski, G. W.; Zamborini, F. P. *J. Am. Chem. Soc.* **2006**, *128*, 5622–5623.
(12) Tsuda, K.; Takeda, Y.; Ogura, H.; Otsubo, Y. *Colloids Surf., A* **2007**, *299*, 262–267.
(13) Yin, J. B.; Zhao, X. P.; Xia, X.; Xiang, L. Q.; Qiao, Y. P. *Polymer* **2008**, *49*, 4413–4419.
(14) Feng, P.; Wan, Q.; Fu, X. Q.; Wang, T. H.; Tian, Y. *Appl. Phys. Lett.* **2005**, *87*, 033114.
(15) Burda, C.; Chen, X. B.; Narayanan, R.; El-Sayed, M. A. *Chem. Rev.* **2005**, *105*, 1025–1102.
(16) Mao, Y.; Park, T. J.; Zhang, F.; Zhou, H.; Wong, S. S. *Small* **2007**, *3*, 1122–1139.
(17) Wang, X.; Zhuang, J.; Peng, Q.; Li, Y. D. *Nature* **2005**, *437*, 121–124.
(18) Lu, K. Q.; Shen, K.; Wang, X. Z.; Sun, G.; Wen, W. J. In *9th International Conference on Electorheological (ER) Fluids and Magnetorheological (MR)*; Beijing, Aug 29—Sept 3, 2004; Lu, K., Shen, R., Liu, J., Eds.; Chinese Academy of Science: Beijing, 2004; pp 3—8.
(19) Shen, R.; Wang, X. Z.; Lu, Y.; Wang, D.; Sun, G.; Cao, Z. X.; Lu, K. Q. *Adv. Mater.* **2009**, *21*, 1–5.
(20) Cheng, Y. C.; Liu, X. H.; Guo, J. J.; Liu, F. H.; Li, Z. X.; Xu, G. H.; Cui, P. *Nanotechnology* **2009**, *20*, 055604.
(21) Rao, A. V. P.; Suresh, M. *Ferroelectrics* **1999**, *229*, 141–146.
(22) Dhage, S. R.; Khollam, Y. B.; Potdar, H. S.; Deshpande, S. B.; Sarwade, B. D.; Date, S. K. *Mater. Lett.* **2002**, *56*, 564–570.
(23) Babko, A. K.; Dubovenko, L. I. *Zh. Neorg. Khim.* **1959**, *4*, 372–378.
(24) Potdar, H. S.; Deshpande, S. B.; Date, S. K. *Mater. Chem. Phys.* **1999**, *58*, 121–127.
(25) Zhao, Z. G.; Geng, F. X.; Bai, J. B.; Cheng, H. M. *J. Phys. Chem. C* **2007**, *111*, 3848–3852.
(26) Estepa, L.; Daudon, M. *Biospectroscopy* **1997**, *3*, 347–369.
(27) Wen, W. J.; Huang, X. X.; Yang, S. H.; Lu, K. Q.; Sheng, P. *Nat. Mater.* **2003**, *2*, 727–730.
(28) Wen, W. J.; Huang, X. X.; Sheng, P. *Soft Matter* **2008**, *4*, 200–210.
(29) Lengalova, A.; Pavlinek, V.; Saha, P.; Stejskal, J.; Kitano, T.; Quadrat, O. *Phys. A* **2003**, *321*, 411–424.
(30) Hao, E.; Schatz, G. C. *J. Chem. Phys.* **2004**, *120*, 357–366.

AM900841M